In silico docking yields small molecule compounds targeting the core of Frizzled 7 as negative allosteric modulators

Supplementary Information

Magdalena M. Scharf[1] Lukas Grätz[1,†] Julia Kinsolving[1] Jan Hendrik Voss[1]

David Carrasco-Busturia[2] Björn Forsberg[3] Peter Kolb[4] Gunnar Schulte[1,*]

[1] Department of Physiology & Pharmacology, Sec Receptor Biology & Signaling, Biomedicum, S-171 65 Stockholm, Sweden

[2] Division of Theoretical Chemistry and Biology, School of Engineering Sciences in Chemistry, Biotechnology and Health, KTH Royal Institute of Technology, SE-100 44 Stockholm, Sweden

[3] Department of Physics, Chemistry and Biology, SciLifeLab, Linköping University, Linköping 58 183, Sweden

[4] Philipps-Universität Marburg, Institute of Pharmaceutical Chemistry, Marburg, Germany

†Current address: Molecular, Cellular and Pharmacobiology Section, Institute of Pharmaceutical Biology, University of Bonn, 53115 Bonn, Germany

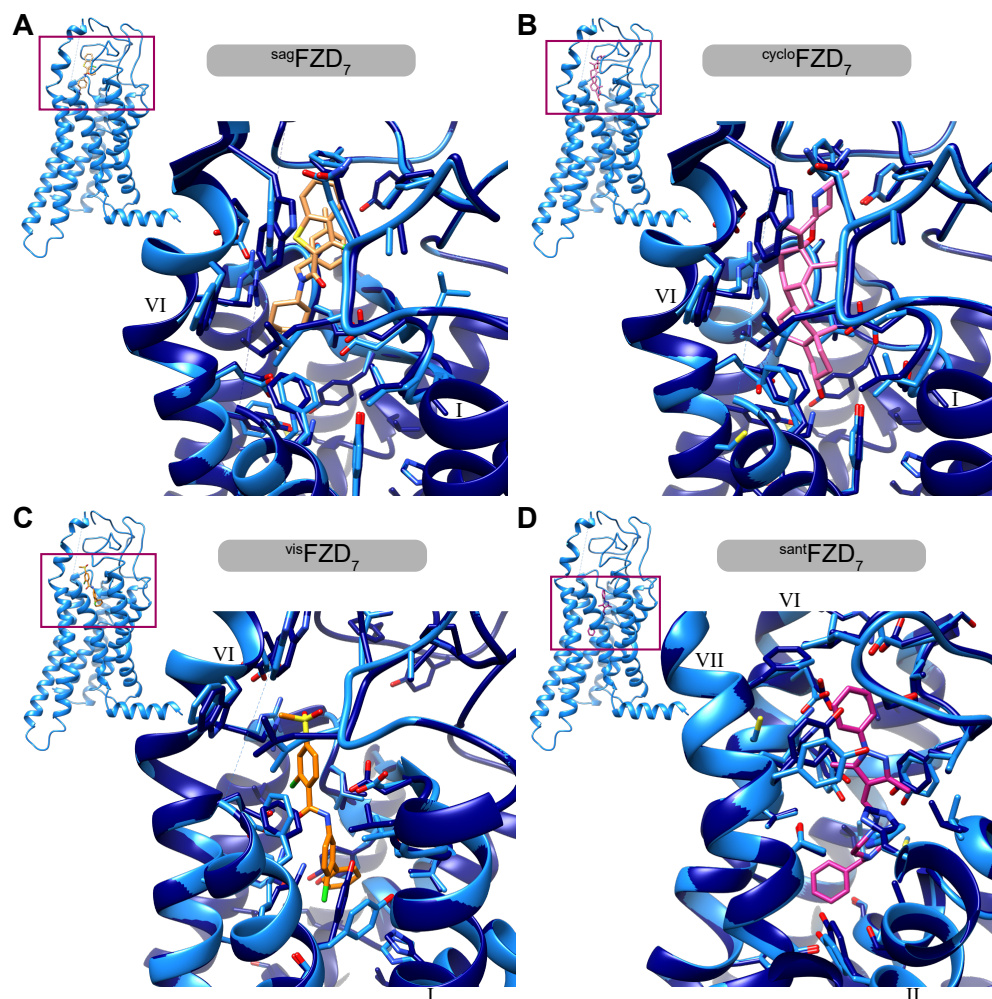*To whom correspondence should be addressed: gunnar.schulte@ki.se

Supplementary Figures

Figure S1: Overview of the prepared docking setups for the initial screen. A: ^{sag}FZD$_7$, B: ^{cyclo}FZD$_7$, C:^{sant}FZD$_7$, D: ^{vis}FZD$_7$. Ligands from SMO structures were merged into the FZD$_7$ structure after alignment. The molecules and residues in 5 Å distance around the molecule were then energy minimised to adapt the artificial binding pocket to binding of a ligand. The side-view of the receptor shows the approximate location of molecule/binding pocket in the 7TMD. Close-up show the comparison of the residues in 5 Å distance around the inserted molecule in the orignal structure 7EVW (dark blue) and after minimising together with the inserted molecule (dodger blue). The respective inserted molecule is highlighted in a different colour (sand: SAG1.5; pink: cyclopamine; orange: vismodegib; violet red: SANT-1). Numbering of the TMs is indicated in roman numerals.
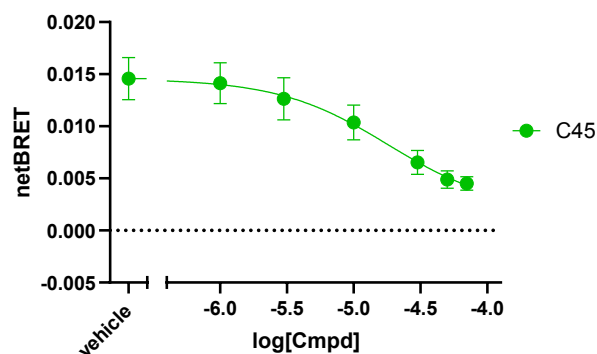
Figure S2: Concentration response curve from BRET-based competition binding experiments with C45 and BODIPY-cyclopamine (Nluc-FZD$_7$). Datapoints are mean $\pm$ SEM of 5 independent experiments.
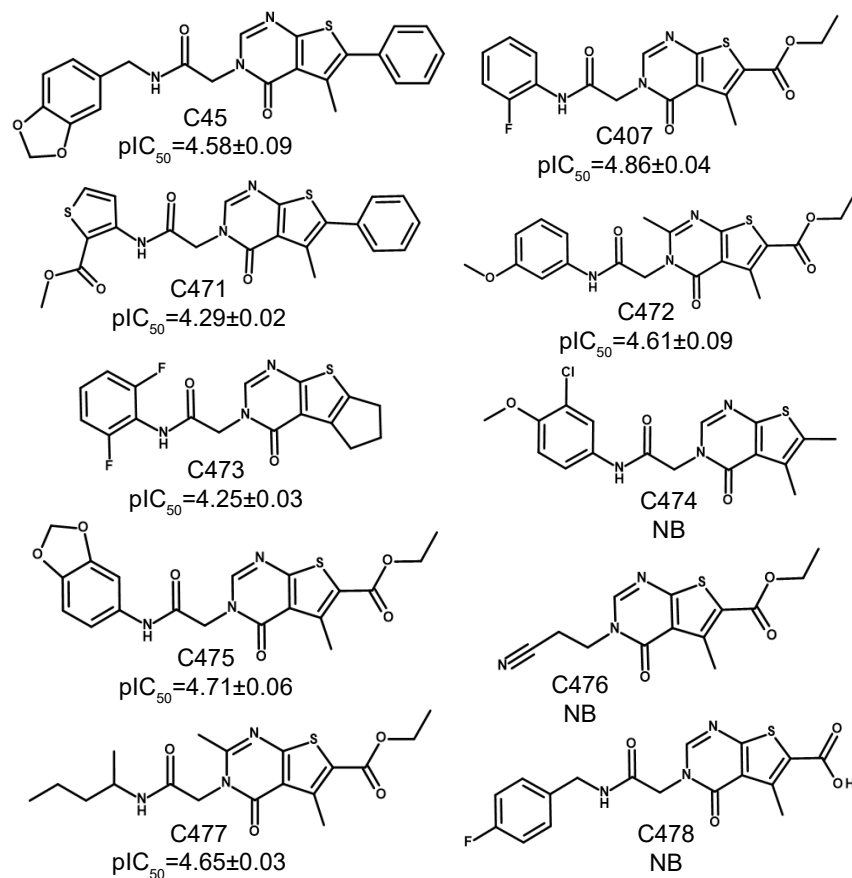

Figure S3: Chemical structures and pIC$_{50}$ values from competition binding experiments for hit molecules C45 and C407 as well as all compounds based on C407 (C471-C478). pIC$_{50}$ are mean $\pm$ SEM for 3-5 independent experiments. NB: Not binding.
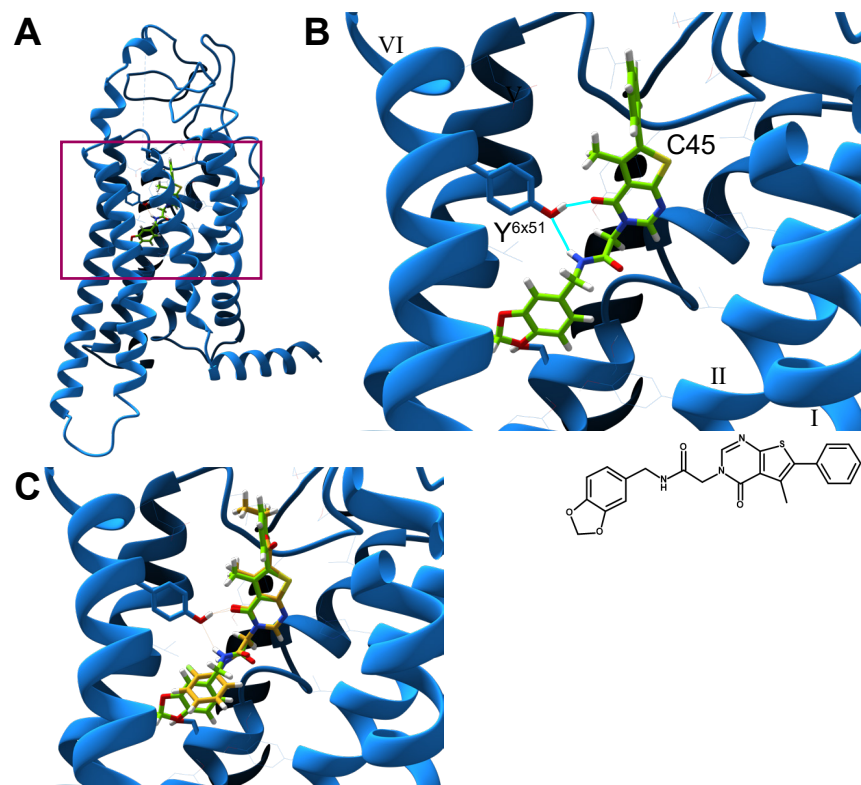
Figure S4: Predicted binding pose of C45 from the docking calculations. A: Side view of the receptor. C45 (bright green) is predicted to bind deep within the 7TMD of FZD_7 (blue), as highlighted by the purple frame. B: Closeup of the predicted binding pose of C45 (bright green) within the receptor core. Compound C45 is predicted to form polar interactions with $Y489^{6x51}$, as indicated by bright blue lines. The chemical structure of C45 is depicted beneath the docking pose for reference. Numbering of the TMs is indicated in roman numerals. C: Overlay of the predicted binding poses of C45 (bright green) and C407 (goldenrod). Both compounds are predicted to bind in a similar pose. B,C: Note that TMs in the front are hidden for better visibility of the compound pose.
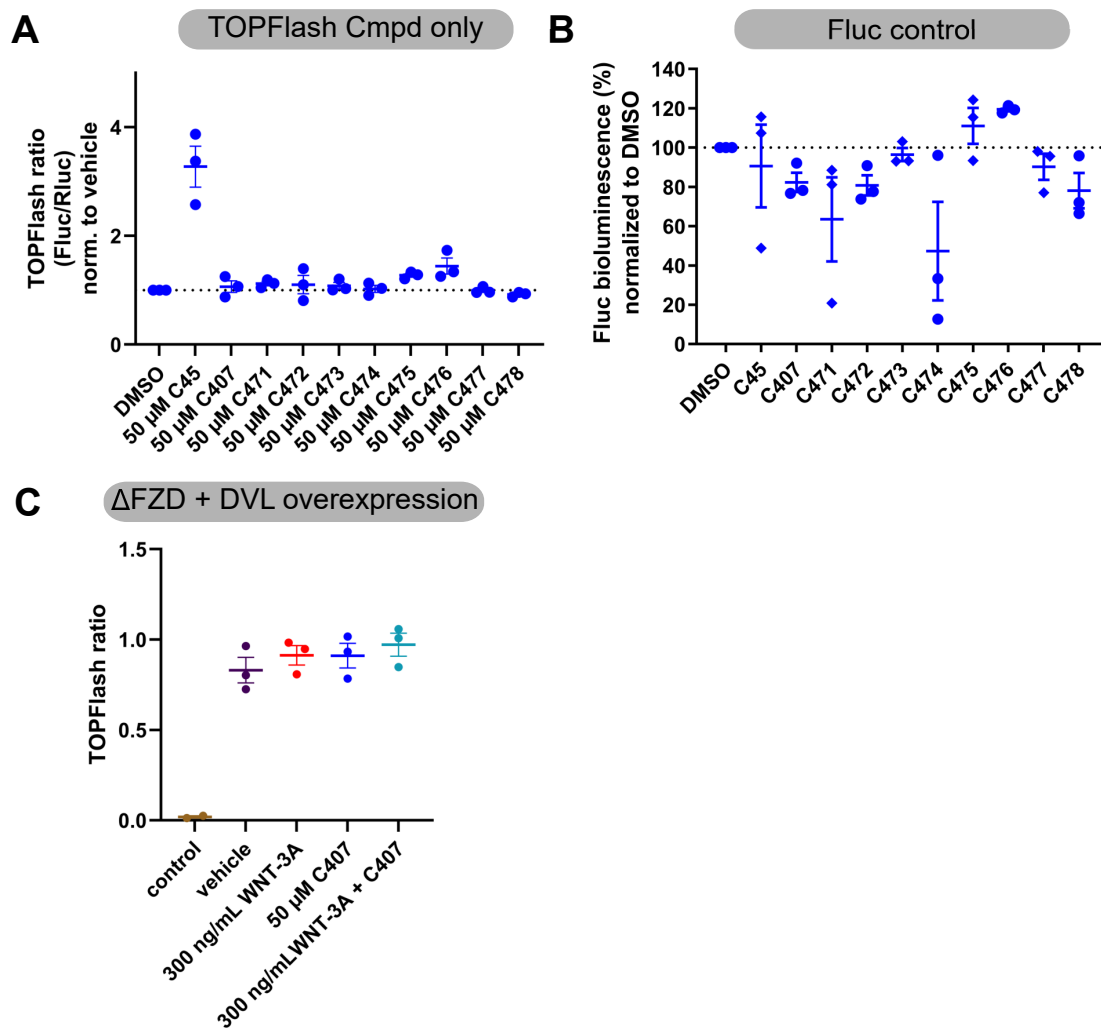
Figure S5: Control experiments for the TOPFlash assay. A: TOPFlash responses induced by the compounds alone at HiBiT-FZD$_7$, which was transfected into ΔFZD$_{1\text{-}10}$ HEK293T cells (no WNT stimulation) B: Control assay to exclude compound-mediated interference with Fluc bioluminescence. Experiments were performed in ΔFZD$_{1\text{-}10}$ HEK293T cells constitutively expressing Fluc. C: Effect of WNT-3A and C407 stimulation on TOPFlash response induced by overexpression of DVL2 in ΔFZD$_{1\text{-}10}$ HEK293T cells. Data points represent means $\pm$ SEM of three independent measurements.
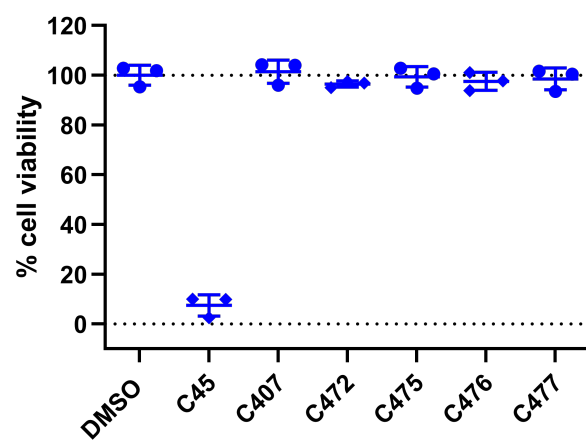
Figure S6: Effect of selected compounds on cell viability of HEK293 cells. Cells were incubated with 10 μM of compound. Data points represent means ± SD of 3 independent measurements.
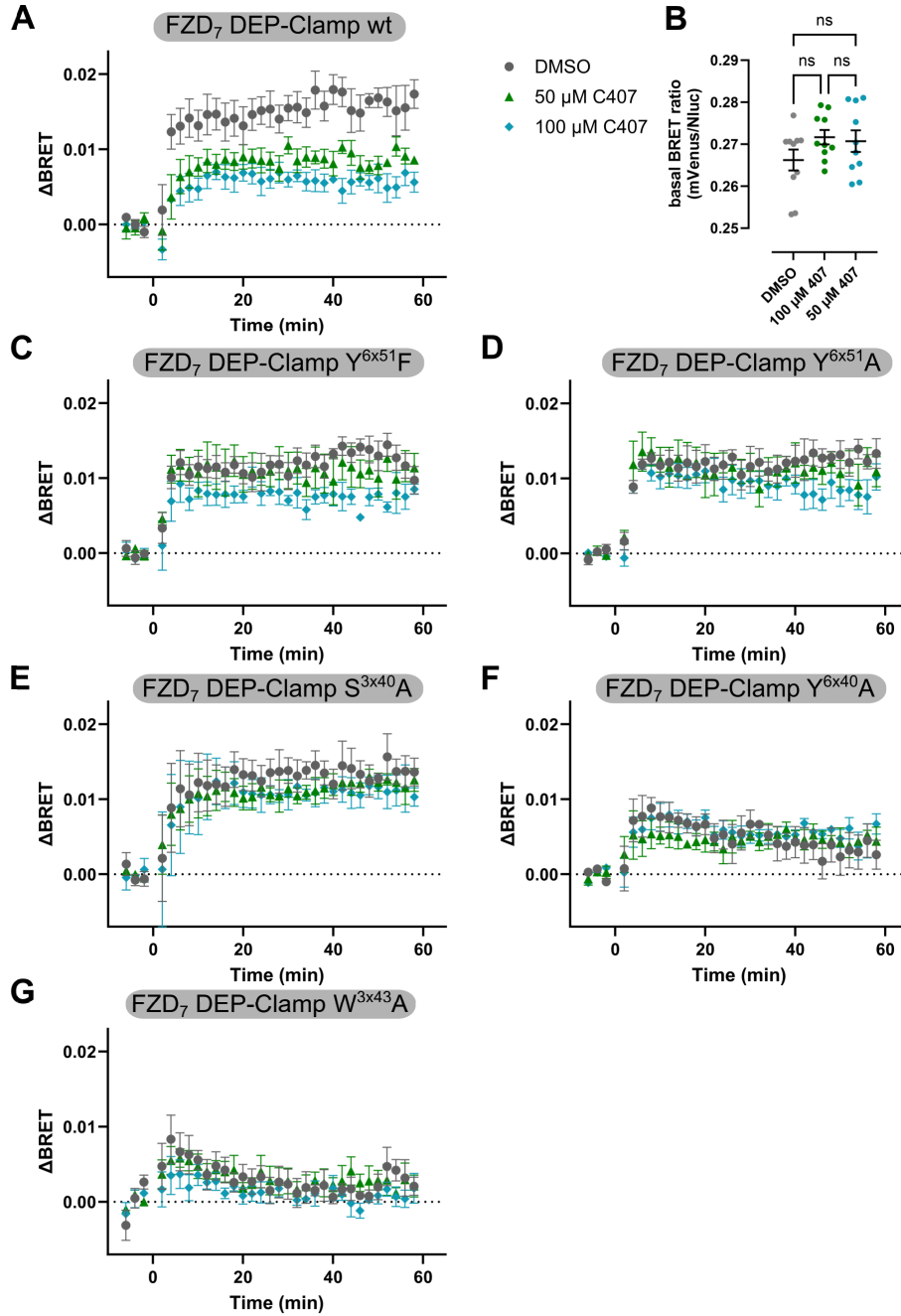
Figure S7: Measurements of BRET changes in the FZD_7-DEP-Clamp sensor. Time-course measurements upon stimulation with WNT-3A only (DMSO; grey circles) and WNT-3A stimulation after pre-incubation with C407 ($50\,\mu M$, green triangles, or $100\,\mu M$, blue squares) are shown for A: wild-type FZD_7; C: FZD_7 $Y489^{6x51}F$; D: FZD_7 $Y489^{6x51}A$; E: FZD_7 $S351^{3x40}A$; F: FZD_7 $Y478^{6x40}A$; and G: FZD_7 $W354^{3x43}A$. In all cases, $1\,\mu g/mL$ WNT-3A was used. Data represent mean $\pm$ SEM for 3-5 independent experiments. B: Basal BRET values for the wild-type FZD_7-DEP-Clamp sensor after pre-incubation with DMSO or C407 only. Data are mean $\pm$ SEM from five independent experiments (technical replicates were averaged for each experiment).
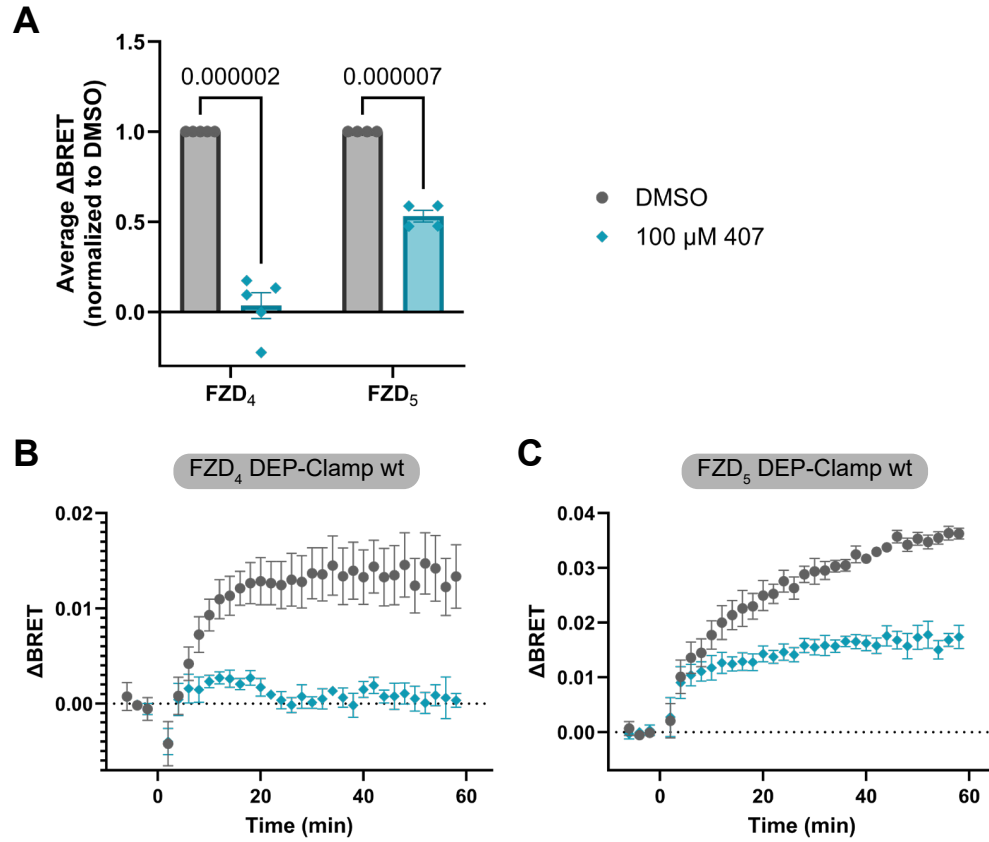
Figure S8: Selectivity measurements of C407 as determined using the FZD$_4$- and FZD$_5$-DEP-Clamp sensors. A: Bar charts showing the average BRET change after stimulation with WNT-3A (1 µg/mL) after pre-incubation with DMSO (grey circles) or C407 (100 µM, blue squares). B, C: Corresponding time-course measurements to A. Data are mean ± SEM for 4-5 independent experiments. Statistical analysis was performed with a multiple unpaired t-test.
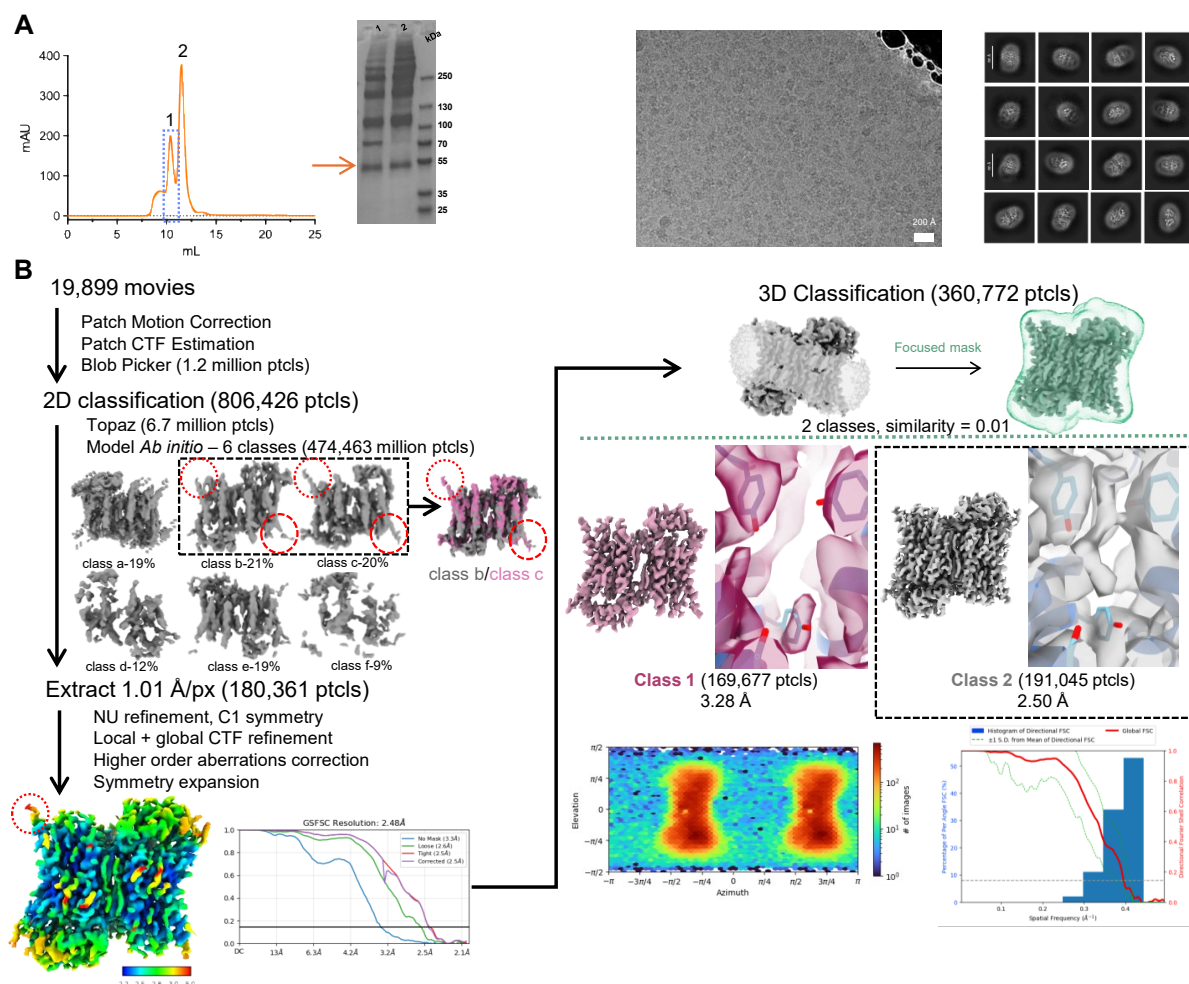
Figure S9: Biochemical characterization and processing pipeline of FZD_7. A: Size exclusion chromatography (SEC) and Coomassie stain of purified FZD_7. The dashed line represents the fraction taken for cryo-EM analysis. A representative micrograph and 2D classifications are taken from the collection. B: The cryo-EM workflow for data processing is detailed. Azimuth plot and FSC curve for the final map are shown. See materials and methods for more details.
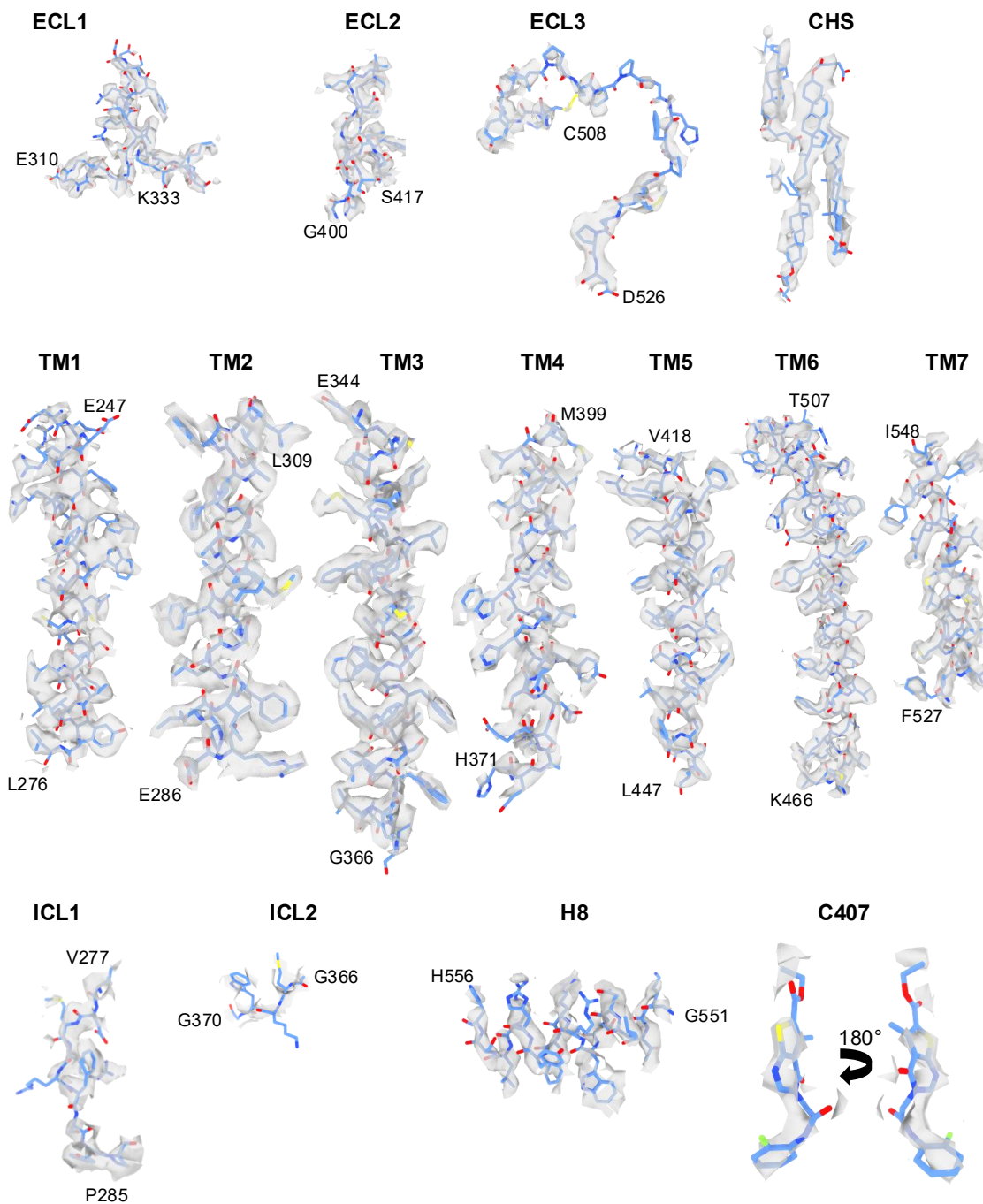
Figure S10: Cryo-EM maps with the model fit of FZD$_7$. The density map of FZD$_7$ is shown with a surface representation (grey) and the contoured map as sticks (blue) for each respective domain, region, molecule or lipid.
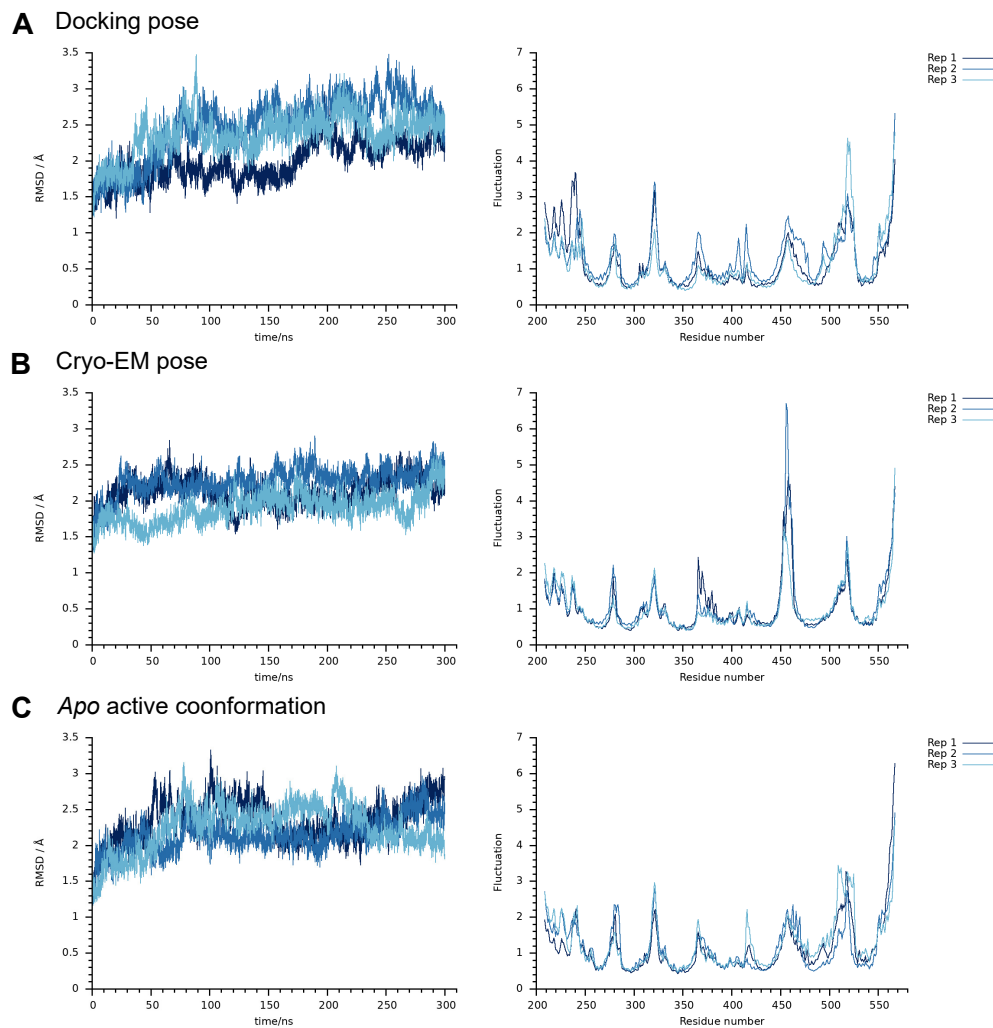
Figure S11: RMSD and RMSF of FZD$_7$ during the MD simulations. Left: Full backbone RMSD of the entire protein and calculated in reference to the initial starting model. Right: RMSF of the full backbone of the protein plotted per residue. A: Starting from the complex of C407 and FZD$_7$ based on the docking calculations. B: Starting from the complex of C407 and FZD$_7$ based on the cryo-EM data. C: Starting from the receptor in an *apo* active conformation as used for the docking calculations. Data for the three independent replica are shown in different shades of blue.

Figure S12: Movement of C407 throughout the trajectories. Left: Starting from the complex of C407 and FZD$_7$ based on the docking calculations. Right: Starting from the complex of C407 and FZD$_7$ based on the cryo-EM data. A: RMSD of C407 heavy atoms in reference to the initial starting pose. B: Distance between C407 'C4' and the D405^{ECL2} Cα atom. C: Distance between C407 'C4' and the Y296^{2x51} Cα atom. D: Distances from B and C plotted against each other. See Supplementary Figure S14 for details on atoms used for the distance measurements. Orange lines and numbers indicate respective distances in the initial starting model. Data for the three independent replica are shown in different shades of blue.

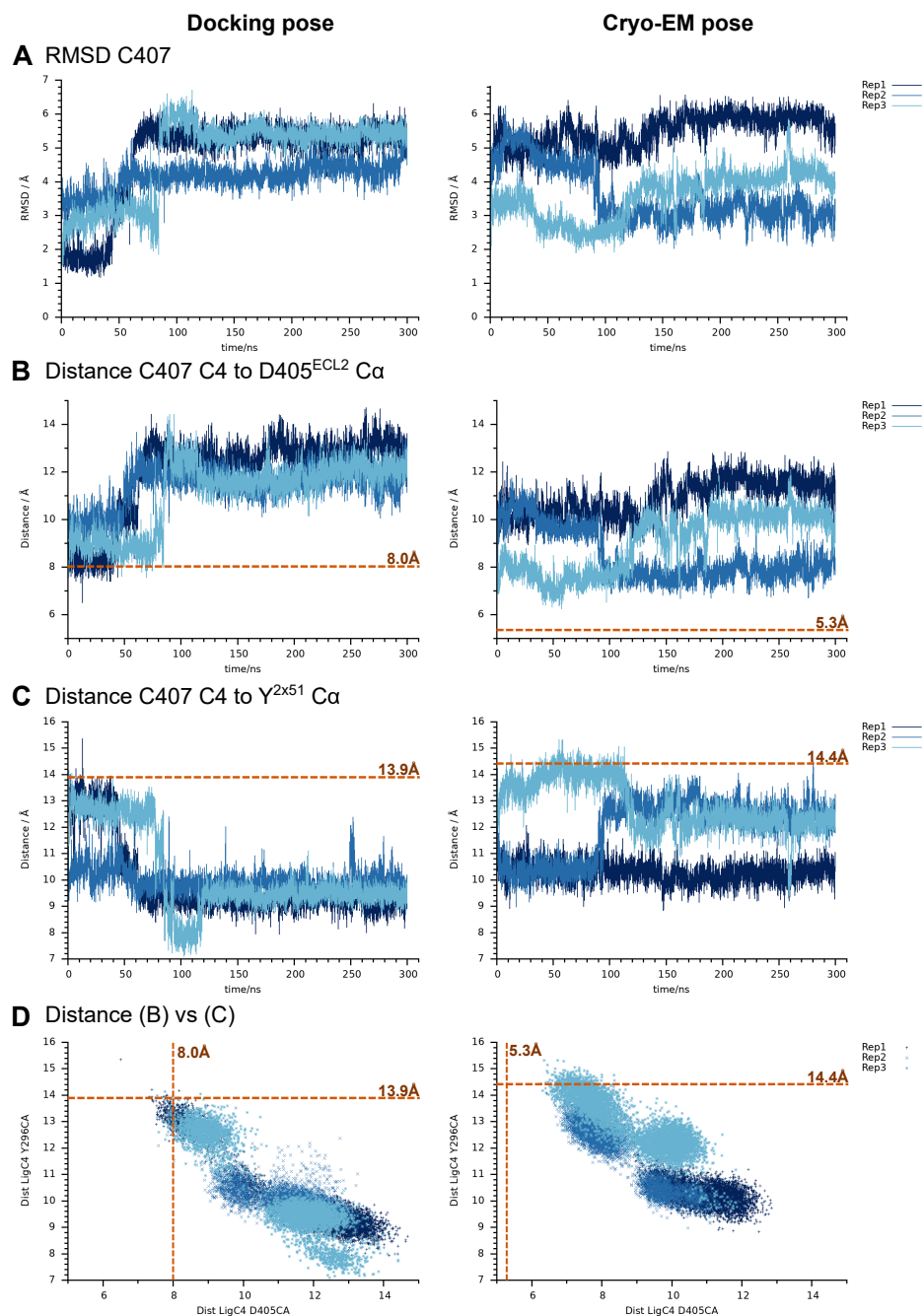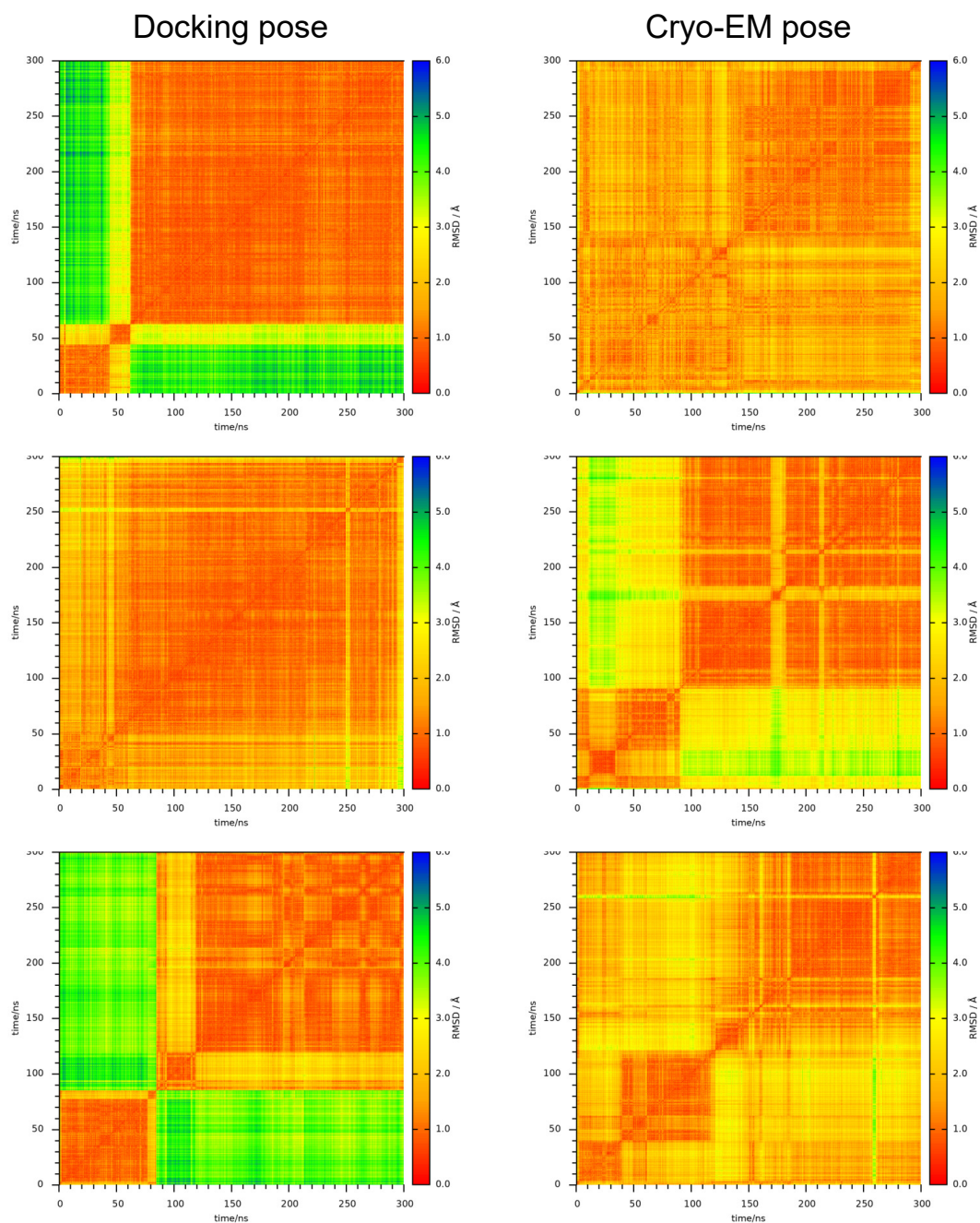Figure S13: 2D-RMS plots of C407 throughout the trajectories. Left: Starting from the complex of C407 and FZD_7 based on the docking calculations. Right: Starting from the complex of C407 and FZD_7 based on the cryo-EM data. Each plot is for one of the three independent replica comparing each frame of the trajectory with each frame of the same trajectory.

A Docking pose
Start pose · Cluster 0 · Cluster 1

B Cryo-EM pose

C Start poses

VI
D405^{ECL2}
Y^{6x51}
S^{3x40}
Y^{2x51}
I

D

C4

fluorophenyl
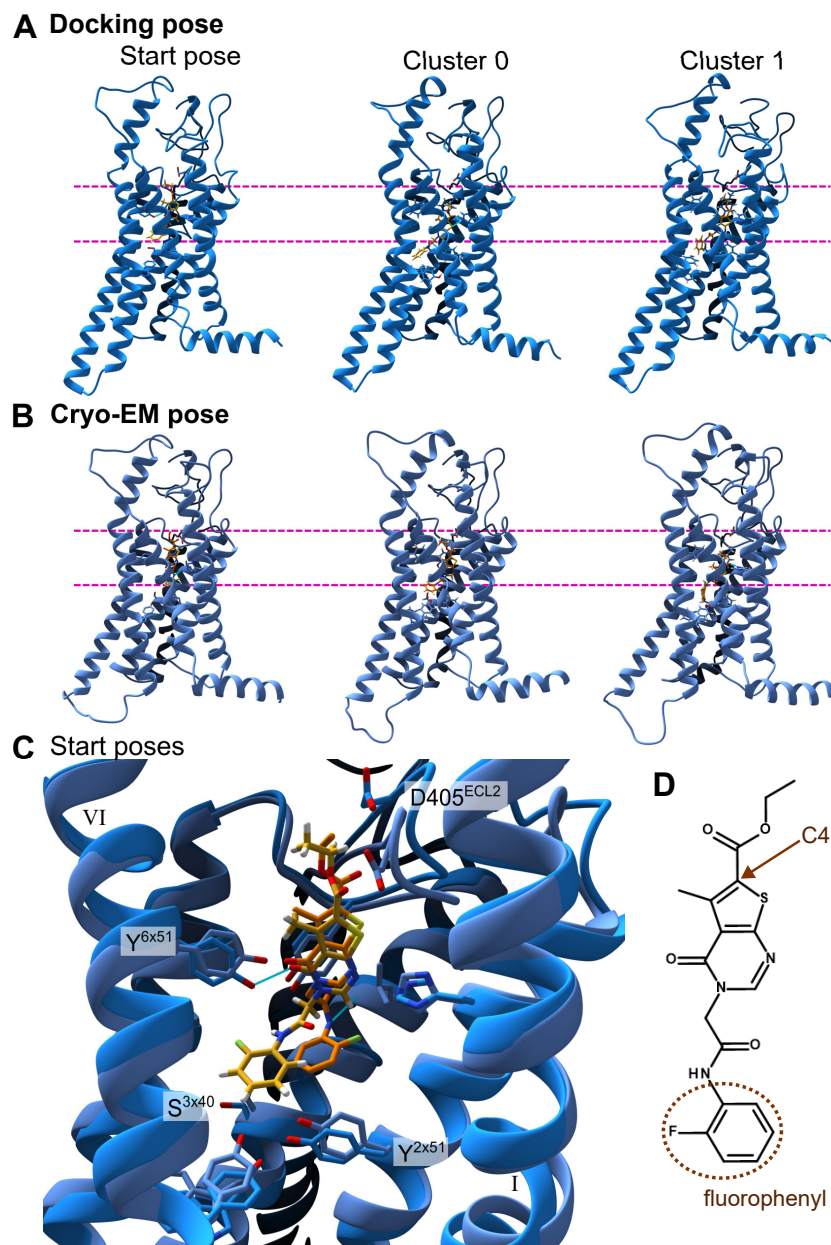
Figure S14: Movement of C407 within the 7TMD throughout the MD simulations and definition of atoms for distance measurements. A: Side-view of the 7TMD of FZD$_7$ for MD simulations starting from the docking pose of C407. Left: Starting pose. Middle: Representative frame of the most frequent pose of C407 during the MD simulation (51 % of frames). Right: Representative frame of the second most frequent pose of C407 (35 % of frames). Pink dashed lines indicate top and bottom reach of C407 within the 7TMD for the initial model. B: Same as A but for the MD simulations starting from the cryo-EM pose. Cluster 0 comprises 56 % of frames and cluster 1 30 %. C: Closeup view of the starting poses of C407 in both MD simulation setups. Residues that were used for distance measurements are indicated with their respective numbering. D: Chemical structure of C407 with moieties and atoms used for distance measurements indicated. Corresponding distance measurements to C and D can be found in Figure 4 and Supplementary Figures S12 and S16.

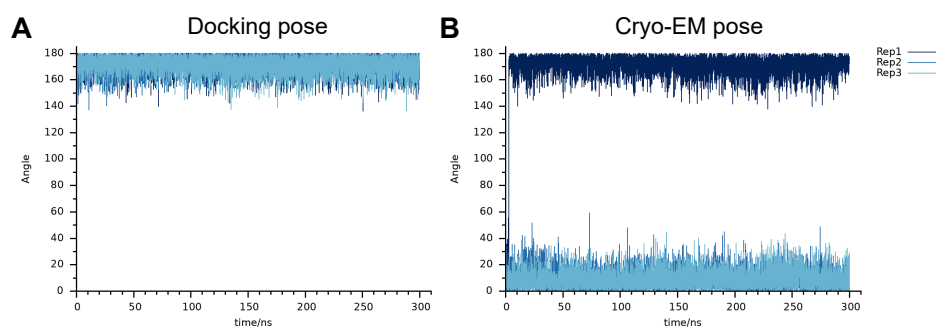Figure S15: Dihedral angle of the amide in C407. A: Starting from the complex of C407 and FZD$_7$ based on the docking calculations. B: Starting from the complex of C407 and FZD$_7$ based on the cryo-EM data. Data of the three independent replica are shown in different shades of blue.
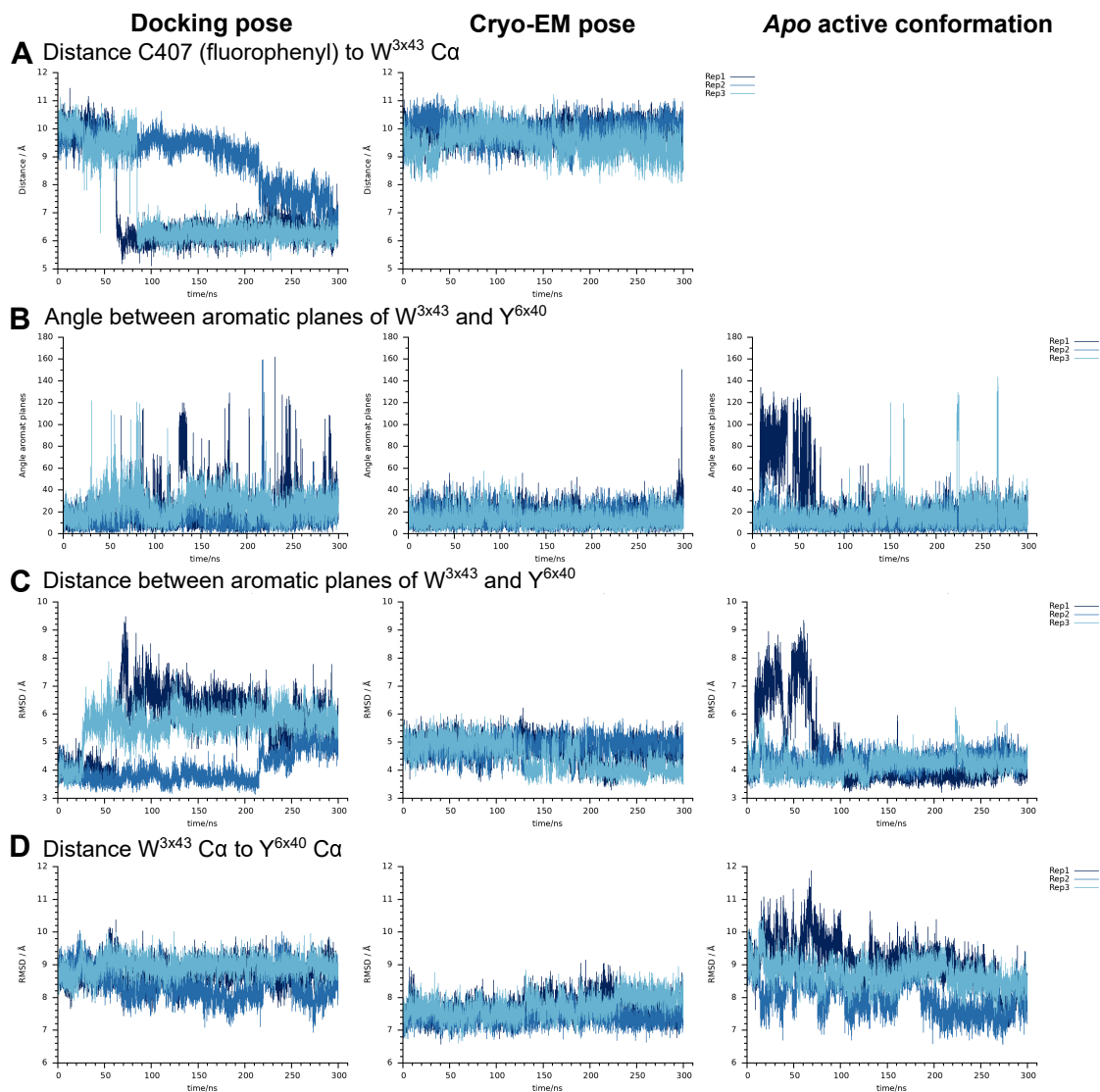
Figure S16: Interplay between the movement of C407 and extended molecular residues W354^{3x43} and Y478^{6x40}. Left: Starting from the complex of C407 and FZD$_7$ based on the docking calculations. Middle: Starting from the complex of C407 and FZD$_7$ based on the cryo-EM data. Right: Starting from the receptor in an *apo* active conformation as used for the docking calculations. A: Distance between the center of mass of the C407 fluorophenyl group (see Supplementary Figure S14) and W354^{3x43} Cα. B: Angle between the vectors perpendicular to the aromatic planes of W354^{3x43} and Y478^{6x40}. C: Distance between the center of mass of the aromat rings of W354^{3x43} and Y478^{6x40}. D: Distance between Cα atoms of W354^{3x43} and Y478^{6x40}. Data for the three independent replica are shown in different shades of blue.

Figure S17: Dihedral angels of the side chain of W354³ˣ⁴³. Left: Starting from the complex of C407 and FZD₇ based on the docking calculations. Middle: Starting from the complex of C407 and FZD₇ based on the cryo-EM data. Right: Starting from the receptor in an *apo* active conformation as used for the docking calculations. A: Dihedral angle between Cα-Cβ-Cγ-Cδ2 atoms of W354³ˣ⁴³. B: Dihedral angle between C-Cα-Cβ-Cγ atoms of W354³ˣ⁴³. C: Dihedral angles from A and B plotted against each other. Orange lines and numbers indicate the respective dihedral angles in the initial starting model. Data of the three independent replica are shown in different shades of blue.
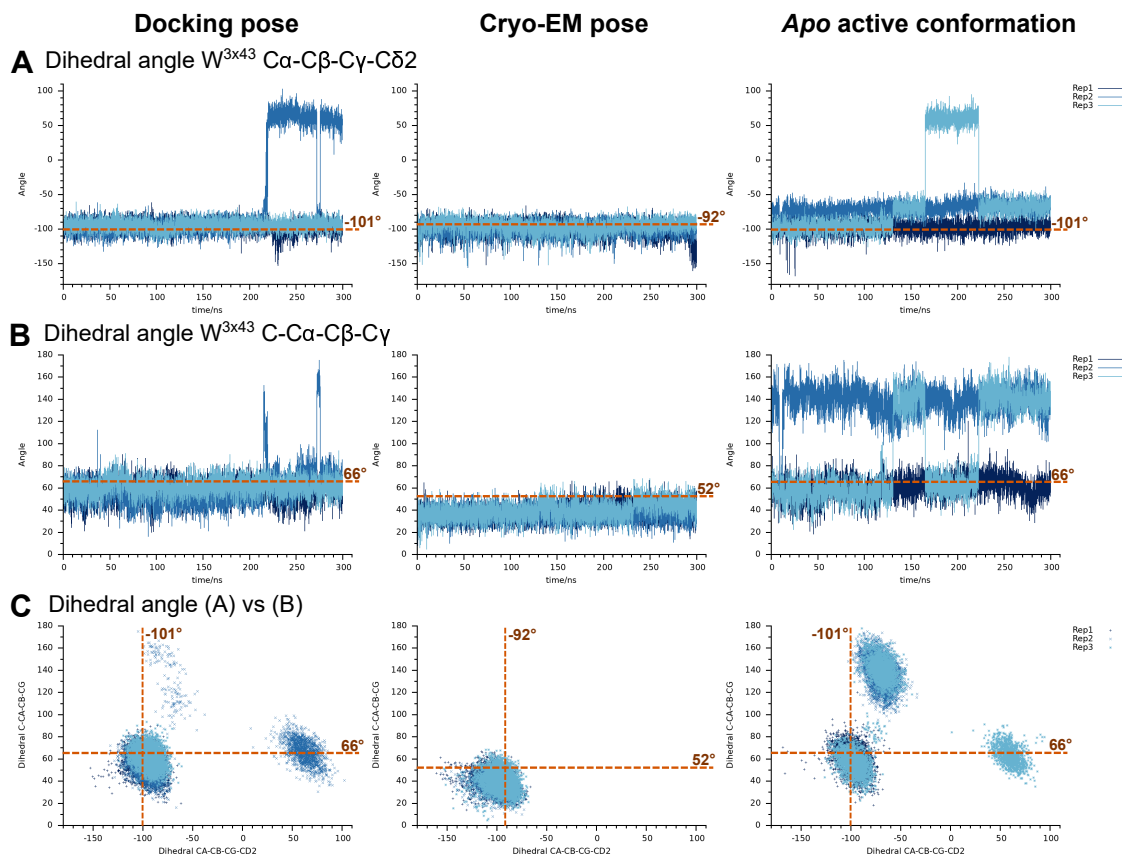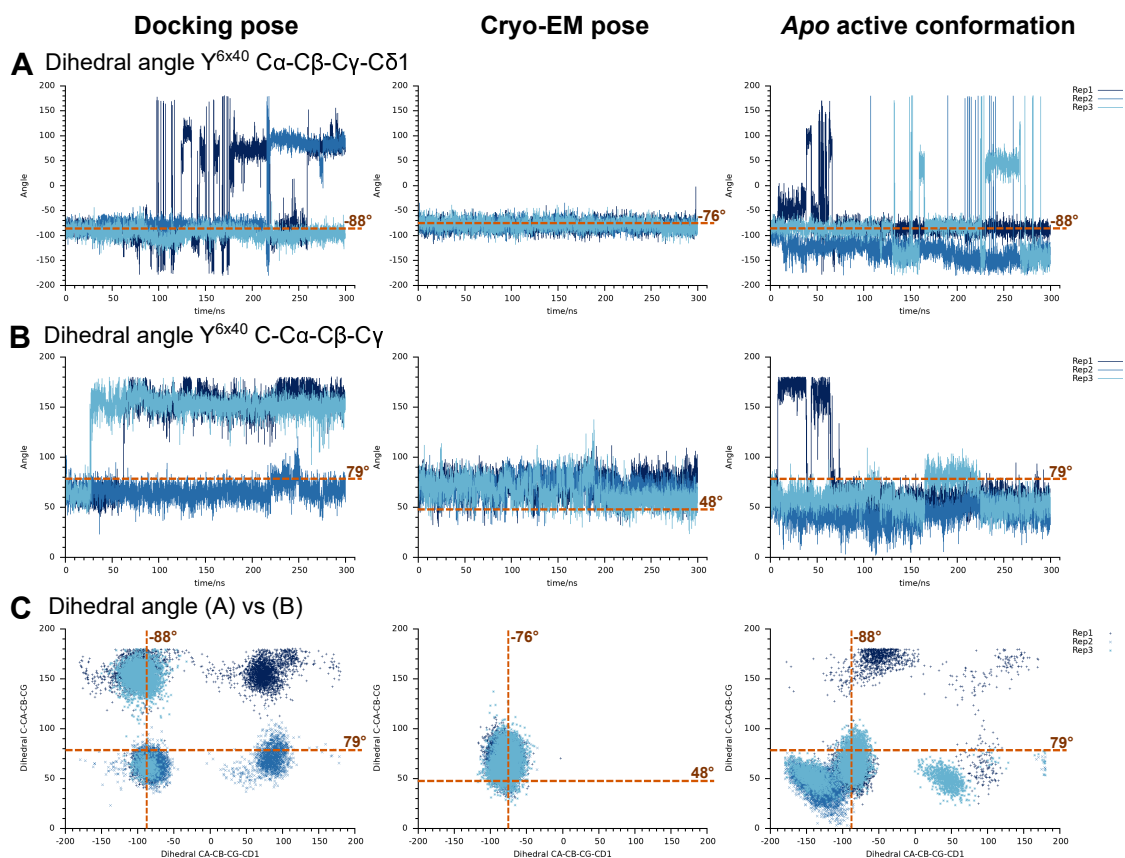
Figure S18: Dihedral angels of the side chain of Y478[6x40]. Left: Starting from the complex of C407 and FZD_7 based on the docking calculations. Middle: Starting from the complex of C407 and FZD_7 based on the cryo-EM data. Right: Starting from the receptor in an *apo* active conformation as used for the docking calculations. A: Dihedral angle between Cα-Cβ-Cγ-Cδ1 atoms of Y478[6x40]. B: Dihedral angle between C-Cα-Cβ-Cγ atoms of Y478[6x40]. C: Dihedral angles from A and B plotted against each other. Orange lines and numbers indicate the respective dihedral angles in the initial starting model. Data of the three independent replica are shown in different shades of blue.

Supplementary Tables

Table S1. Cryo-EM data collection, refinement, and validation statistics.

	EMDB-53969/ PDB: 9RHG
Data collection and processing	
Magnification	165,000
Voltage (kV)	300
Defocus range (μM)	-0.4 -1.8
Pixel size (Å)	0.507
Symmetry imposed	C1
Initial particle images (no.)	19,899
Map resolution	
FSC threshold	0.143
Map local resolution range (Å)	2.13-3.43
Refinement	
Initial models used	9EPO
Model resolution (Å) (FSC=0.143)	1.9
Map sharpening B factor (Å^2)	-30
Model composition	
Non-hydrogen atoms	5767
Number of protein residues/atoms	694
Number of ligands/ligand atoms	5
Average B factor (Å^2)	
Protein	51.37
Ligands	34.83
R.m.s deviations	
Bond lengths (Å)	0.003

Continuation of Table S1.

	EMDB-53969/ PDB: 9RHG
Bond angles (°)	0.669
Validation	
Molprobity score	1.35
Clashscore	3.91
Poor rotamers (%)	1.69
Ramachandran plot	
Favored (%)	98.25
Allowed (%)	1.75
Disallowed (%)	0

EMD; electron microscopy bank, PDB; protein data bank, RMSD; root mean square deviation.

Table S2. System setup parameters for all included MD simulations.

	apo active	Docking pose	Structure pose
Simulation box dimensions	85 x 85 x 120	85 x 85 x 120	85 x 85 x 120
Total number of atoms	71288	71352	70425
Number of water molecules	15198	15205	14852
Salt concentration [mM]	150	150	150
Lipid composition			
Lipid type	POPC	POPC	POPC
Number of lipids (Top layer)	75	75	75
Number of lipids (Bottom layer)	73	73	74
Simulation length			
Equilibration *NVT* [ns]	0.25	0.25	0.25
Equilibration *NPT* [ns]	16.75	16.75	16.75
Production runs [ns]	300	300	300
Number of replica	3	3	3

Table S3. Vendor and compound identifiers for all tested compounds as well as compound purities as provided by vendor quality control data. The hit molecules identified in pharmacological assays are highlighted in grey.

ID	ZINC ID	MolPort ID	Vendor ID	Vendor	purity
C11	ZINC000006069641		sc-210120B	SantaCruz	≥95%
C12	ZINC000065408474	MolPort-047-489-699	53943877	ChemBridge	100%
C13	ZINC000072126504	MolPort-047-494-752	16054903	ChemBridge	93%
C14	ZINC000072419084	MolPort-047-495-109	34193291	ChemBridge	97%
C15	ZINC000077321841	MolPort-047-497-053	23318776	ChemBridge	100%
C16	ZINC000163762760		Z1515110521	Enamine	97%
C17	ZINC000328654785		Z1757898504	Enamine	95%
C21	ZINC000006702107	MolPort-000-832-620	9019362	ChemBridge	≥85%
C22	ZINC000097604206	MolPort-047-503-159	57305870	ChemBridge	94%
C31	ZINC000000812166		Z46168873	Enamine	100%
C32	ZINC000067805280	MolPort-019-816-663	70332011	ChemBridge	100%
C33	ZINC000067934644	MolPort-019-821-985	87464791	ChemBridge	95%
C34	ZINC000072898705		Z1301343910	Enamine	96%
C35	ZINC000095421423		Z1439375842	Enamine	98%
C36	ZINC000151702594		Z1458340850	Enamine	100%
C37	ZINC000178964316		Z2242915358	Enamine	100%
C38	ZINC000244787808	MolPort-039-034-783	16750652	ChemBridge	100%
C41	ZINC000000142135	MolPort-000-662-104	6541524	ChemBridge	≥85%
C42	ZINC000000618889	MolPort-001-580-765	STK149302	Vitas-M	≥85%
C43	ZINC000005685988	MolPort-001-558-552	7657461	ChemBridge	≥85%
C44	ZINC000013127563	MolPort-002-597-530	STL221649	Vitas-M	≥85%
C45	ZINC000014128943		Z88129578	Enamine	89%
C401			CBK448805	CBCS library	98%

Continuation of Table S3.

ID	ZINC ID	MolPort ID	Vendor ID	Vendor	purity
C402			CBK413891	CBCS library	99%
C403			CBK249809	CBCS library	94%
C404			CBK071900	CBCS library	99%
C405			CBK268514	CBCS library	94%
C406			CBK072830	CBCS library	93%
C407[a]			CBK434718	CBCS library	98%
C407			Z25040997	Enamine	100%
C408			CBK304562	CBCS library	85%
C409			CBK449777	CBCS library	98%
C410			CBK297102	CBCS library	55%
C411			CBK071910	CBCS library	99%
C471			Z202575498	Enamine	94%
C472			Z94735417	Enamine	98%
C473			Z87739603	Enamine	94%
C474			Z26743350	Enamine	94%
C475			Z25040877	Enamine	94%
C476			Z54342035	Enamine	100%
C477			Z94736991	Enamine	97%
C478			Z107063344	Enamine	93%

[a] C407 from this source was only used for initial binding experiments. All other experiments were conducted with C407 from Enamine.

Table S4. Compound SMILES for all tested compounds.

ID	SMILES
C11	Cc1cc(=O)oc2cc(OC(=O)c3ccc(N=C(N)N)cc3)ccc12
C12	O=C(N(Cc1ccc(F)cc1)Cc1ccccn1)C12CNCC1CNC2
C13	CN(Cc1nc(-c2ccccc2)no1)C(=O)[C@H]1CC2(CCNCC2)CN1
C14	Cc1ccc(OCCNC[C@]2(O)CCCNC2)cc1C
C15	O[C@]1(CNCc2ccc(-n3cccn3)cc2)CNCCOC1
C16	NCC[C@H]1CCCN(Cc2ccc(F)c(C(F)(F)F)c2)C1
C17	CN1CC[C@@H](CNCc2cccc3nccn23)[C@@H]1c1cccnc1
C21	Brc1ccc(OCc2ccccc2)c(CNCc2cccnc2)c1
C22	NCC[C@H]1CN(Cc2ccc(Oc3ccccc3)cc2)CCO1
C31	O=C(CN1CCCC1)Nc1ccc(Br)cc1
C32	Cc1ccc(O)c(CN2CCC([C@]3(c4cccnc4)NC(=O)NC3=O)CC2)c1
C33	COc1ccc(Oc2nc(C)cnc2C)cc1CN1CCCC1
C34	Cc1ccc(NC(=O)CN2CCC3(CCOCC3)C2)cc1
C35	O=C(Nc1ccc(CN[C@@H]2CCc3ccccc32)cc1)c1cccnc1
C36	O=C(CNC[C@H]1CCCO1)Nc1ccc(-c2csnn2)cc1
C37	CNC[C@@H]1CCN(C(=O)[C@H]2COc3ccc(Cl)cc3C2)C1
C38	O=C(CN1CCC2(CC1)c1ccccc1C[C@H]2O)Nc1ccc(F)cc1
C41	Cc1ccc(N2C(=O)C(Cl)=C(Nc3cccc(O)c3)C2=O)c(C)c1
C42	CCOc1cccc(N2C(=O)C[C@H](n3cnc4ccccc43)C2=O)c1
C43	COC(=O)c1ccc(NC(=O)CSc2nc(CC(C)C)n[nH]2)cc1
C44	COc1ccc([C@@H]2C[C@H](c3ccc(C)cc3)Nc3nc(N)nn32)cc1
C45	Cc1c(-c2ccccc2)sc2ncn(CC(=O)NCc3ccc4c(c3)OCO4)c(=O)c12
C401	s1c2ncn(c(=O)c2cc1c1ccccc1)CC(=O)OCCC
C402	s1c2ncn(c(=O)c2c2c1CCCC2)CC(=O)NCc1ccccc1
C403	c12c(ncn(c1=O)CC(=O)NCCOc1cc(Cl)ccc1)sc(c2C)C

Continuation of Table S4.

ID	Smiles
C404	c12c(ncn(c1=O)CC(=O)NCc1ncccc1)sc(c2)C
C405	c12c(sc(c1C)C(=O)N)ncn(c2=O)CC(=O)NCCc1ccccc1
C406	n1(c(=O)c2c(nc1C)cccc2)CC(=O)NCc1ccccc1
C407	s1c2ncn(c(=O)c2c(c1C(=O)OCC)C)CC(=O)Nc1c(F)cccc1
C408	c12c(ncn(c1=O)CC(=O)NC1c3c(OCC1)cccc3)sc(c2C)C
C409	s1c2ncn(c(=O)c2c(c1C(=O)N)C)CC(=O)Nc1c(cccc1)CC
C410	c12c(ncn(c1=O)CC(=O)c1cc3c(OCO3)cc1)sc(c2)c1ccccc1
C411	c12c(sc(c1C)C(=O)Nc1c(OC)cccc1)ncn(c2=O)CC(=O)NCCC
C471	Cc1c(-c2ccccc2)sc(N=CN2CC(Nc3c(C(OC)=O)scc3)=O)c1C2=O
C472	CCOC(c1c(C)c(C(N(CC(Nc2cc(OC)ccc2)=O)C(C)=N2)=O)c2s1)=O
C473	O=C(CN(C=Nc1c2c(CCC3)c3s1)C2=O)Nc(c(F)ccc1)c1F
C474	Cc1c(C)sc(N=CN2CC(Nc(cc3)cc(Cl)c3OC)=O)c1C2=O
C475	CCOC(c1c(C)c(C(N(CC(Nc(cc2)cc3c2OCO3)=O)C=N2)=O)c2s1)=O
C476	CCOC(c1c(C)c(C(N(CCC#N)C=N2)=O)c2s1)=O
C477	CCCC(C)NC(CN(C(C)=Nc1c2c(C)c(C(OCC)=O)s1)C2=O)=O
C478	Cc1c(C(O)=O)sc(N=CN2CC(NCc(cc3)ccc3F)=O)c1C2=O